BLOOFINZ - Gulf of Mexico

Microbial food web dynamics in the oceanic Gulf of Mexico

MICHAEL R. LANDRY[1],*, KAREN E. SELPH[2], MICHAEL R. STUKEL[3], RASMUS SWALETHORP[1], THOMAS B. KELLY[3], JENNIFER L. BEATTY[4] AND CAMERON R. QUACKENBUSH[5]

[1]SCRIPPS INSTITUTION OF OCEANOGRAPHY, UNIVERSITY OF CALIFORNIA, DAN DIRGO, 9500 GILMAN DR., LA JOLLA, CA 92093-0227, USA, [2]DEPARTMENT OF OCEANOGRAPHY, UNIVERSITY OF HAWAII AT MANOA, 1000 POPE ROAD, HONOLULU, HI 96822, USA, [3]EARTH, OCEAN AND ATMOSPHERIC SCIENCE, FLORIDA STATE UNIVERSITY, 0100 ACADEMIC WAY, TALLAHASSEE, FL 32306-4520, USA, [4]DEPARTMENT OF BIOLOGICAL SCIENCES, UNIVERSITY OF SOUTHERN CALIFORNIA, 3616 TROUSDALE PARKWAY, LOS ANGELES, CA 90089-0371, USA AND [5]MOSS LANDING MARINE LABORATORIES, SAN JOSÉ STATE UNIVERSITY, MOSS LANDING, CA 95039, USA

*CORRESPONDING AUTHOR: mlandry@ucsd.edu

Phytoplankton growth and microzooplankton grazing rates were measured in repeated profiles of dilution experiments incubated *in situ* on a drift array in order to assess microbial production and food web characteristics in the oligotrophic bluefin tuna spawning habitat of the Gulf of Mexico (May peak spawning seasons, 2017–2018). Grazing often exceeded growth with the processes more balanced overall in the surface mixed layer, but biomass accumulated in the mid-euphotic zone. Community production estimates (260–500 mg C m^{-2} day^{-1}) were low compared to similar open-ocean studies in the Pacific Ocean. *Prochlorococcus* was a consistent major contributor (113–204 mg C m^{-2} day^{-1}) to productivity, while diatoms and dinoflagellates (2–10 and 4–13 mg C m^{-2} day^{-1}, respectively) were consistently low. Prymnesiophytes, the most dynamic component (34–134 mg C m^{-2} day^{-1}), co-dominated in 2017 experiments. Unexpected imbalances in grazing relative to production were observed for all picoplankton populations (*Prochlorococcus*, *Synechococcus* and heterotrophic bacteria), suggesting a trophic cascade in the absence of mesozooplankton predation on large microzooplankton. Study sites with abundant larval tuna had the shallowest deep chlorophyll maxima and significant net positive phytoplankton growth below the mixed layer.

KEYWORDS: phytoplankton growth; production; microzooplankton grazing; picoplankton; *Prochlorococcus*; prymnesiophytes; diatom; dinoflagellates; heterotrophic bacteria

INTRODUCTION

Microbial food web dynamics—comprising the growth and mortality interactions of protists and bacteria—generate and consume most of the ocean's productivity (Rivkin and Legendre, 2001; Calbet and Landry, 2004) and drive the biological responses to variable physical forcing that underlie temporal and spatial patterns in biomass, composition and function. In the Gulf of Mexico (GoM), experimental studies of microbial growth and grazing, done mainly with near-surface samples from shallow estuaries or coastal shelf stations, have revealed massive process variability on seasonal scales (Murrell *et al.*, 2002), over salinity and oxygen gradients (Fahnenstiel *et al.*, 1995; Jochem, 2003; Liu and Dagg, 2003), in thin layers (Greer *et al.*, 2020), among taxa and size classes (Strom and Strom, 1996; Jochem, 2003; Juhl and Murrell, 2005; First *et al.*, 2009), in response to nutrient loading and limitation (Strom and Strom, 1996; Juhl and Murrell, 2005), and as a consequence of harmful algal blooms and other factors (First *et al.*, 2007). By contrast, microbial food web dynamics are almost entirely unexplored in oceanic oligotrophic waters of the GoM, which remains an obstacle for understanding how that system functions ecologically as a nutritional habitat, how it compares to other open-ocean regions, and what its baseline characteristics and vulnerabilities might be to future human-caused perturbations, like oil spills and climate change.

The present experimental study was done as part of the BLOOFINZ-GoM (Bluefin Larvae in Oligotrophic Ocean Foodwebs, Investigations of Nitrogen to Zooplankton) Project, which combined approaches of fisheries oceanography and lower-level food web ecology in assessing habitat quality for the larvae of Atlantic bluefin tuna (ABT) in the oceanic GoM (Gerard *et al.*, this issue). Sampling was guided by an adaptive habitat model that predicted areas, such as the outer edges of Loop Current eddies, where ABT larvae would be concentrated (Muhling *et al.*, 2010; Domingues *et al.*, 2016). We expected that such habitats would be less variable dynamically than the coastal GoM and show balanced growth and grazing processes, especially for picoplankton. Additional major a priori questions were how these study sites compare to other open-ocean systems in terms of magnitudes and group-specific distributions of production and grazing and whether they exhibit specific characteristics, such as subsurface blooms of large phytoplankton (e.g. Landry *et al.*, 2008), that might enhance the efficiency of trophic coupling to ABT larvae. To address such questions, our study involved elements that have not been done previously in the GoM: (i) integrated process measurements over the extended euphotic zone, (ii) *in situ* incubations under ambient light and temperature conditions, (iii) resolved group-specific contributions to carbon production and grazing and (iv) measured net rates of change of the ambient microbial community to compare against experimental determinations of process rates.

METHODS

Sampling and experimental setup

Microplankton community standing stocks and process rates were investigated in the Gulf of Mexico during two BLOOFINZ-GoM cruises on NOAA Ship *Nancy Foster* in 2017 (NF1704, 7 May–2 June) and 2018 (NF1802, 27 April–20 May). Experimental locations were guided by the habitat index model of Domingues *et al.* (Domingues *et al.*, 2016) based on real-time satellite imagery and by site survey sampling for ABT larvae (Gerard *et al.*, this issue). On each cruise, we conducted multi-day quasi-Lagrangian experiments, called "cycles," during which we sampled and measured processes on a repeated daily schedule following a satellite-tracked free-drifting array (Landry *et al.*, 2009). The drift array (Pacific Gyre, San Diego) consisted of a surface float, a 3-m drogue centered at 15 m, coated wire with stainless-steel attachment rings for *in situ* bottle incubations, and a separately attached smaller float with iridium transmission (10-min position frequency) and nighttime strobe light. Five cycle experiments were conducted on the two cruises (Fig. 1). Our analysis focuses on Cycle 1 (C1), a 3-day experiment in 2017, and Cycles 4 and 5 (C4, C5), both 4-day experiments in 2018. We also present some combined results for C2 and C3, which sampled different points of an eddy feature in 2017, but microscopical and HPLC pigment data for those experiments are insufficient for full comparative analyses.

For each experiment, we collected seawater daily from Niskin bottles on early-morning CTD hydrocasts (∼02:00 local time) at six depths, ranging from 5 m to the deep chlorophyll maximum (DCM) in the euphotic zone defined by the depth of penetration of 1% surface irradiance. Samples for initial concentrations of pigments, flow cytometry (FCM) and microscopy were filled directly from the Niskin bottles via silicone tubing. For each depth, we also prepared a dilution experiment that compared net population growth rates in polycarbonate bottles (2.7 L) containing unfiltered seawater (100%) and a dilution treatment consisting of ∼32% whole seawater diluted with filtered seawater from that depth (Landry *et al.*, 2008, 2011b). Seawater was filtered directly from the Niskin bottles using a peristaltic pump, silicone tubing and an in-line 0.2 μm Suporcap filter capsule that had
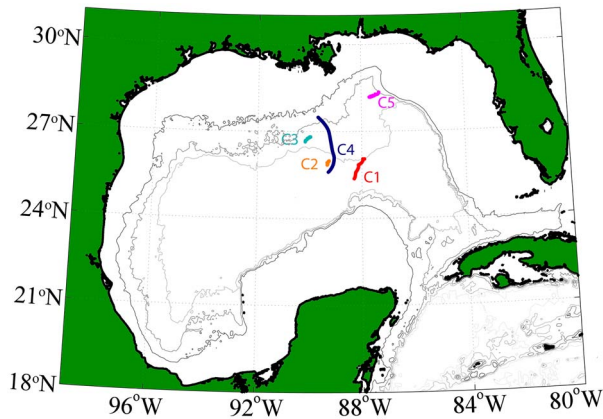
Fig. 1. Map of experimental study site in the Gulf of Mexico. Traces depict drift trajectories of Cycles 1–5. Cycle numbers are closest to the locations of drifter deployments.

previously been acid washed (3.7% trace-metal grade HCl; Milli-Q and seawater rinses). Dilution bottles were first given a measured volume of filtered water and then gently filled to the top with water from the Niskin bottles. The fill water was unscreened to avoid physical damage to fragile protists (Gifford, 1988; Lessard and Murrell, 1998). Consistent with previous studies with the two-treatment method in open-ocean systems (Landry *et al.*, 2008, 2009, 2011a, b, 2016b), we also did not add nutrients to the incubation bottles. Lessard and Murrell (Lessard and Murrell, 1998) demonstrated that added nutrients were not needed for reasonable rate estimates and linearity in dilution experiments conducted in the oligotrophic Sargasso Sea, whereas adding nutrients resulted in erratic results and depressed grazing. After preparation, each bottle was subsampled for FCM analysis (2 mL) for initial concentrations and volumetric dilution factors. In addition to the dilution experiment bottles, we filled triplicate 2.8-L polycarbonate bottles at each depth (and a 2.8-L "dark" bottle) and spiked them with $H^{13}CO_3^-$ to measure net primary productivity (NPP, for additional details see Yingling *et al.*, 2021).

All bottles were secured into coarse net bags with top and bottom attachment clips and incubated *in situ* for 24 h at the depth of collection on the line below the drifter float. For the first deployment of each cycle, the entire array with bottles attached was laid out on deck before being quickly lowered by hand. For subsequent daily experiments, a new 6-depth experiment was set up in net bags on deck before recovering the drifter. The drifter was then recovered, the previous day's experiments were removed, the new experiments were attached, and the drifter was redeployed—a process that took ~15 min while the ship maintained position. All recovery and deployments were carried out before sunrise. Sampling for daily experiments was done in close

proximity (~100 m) to the drifter position. Upon recovery, all bottles were subsampled for assessments of community composition and biomass, as described below.

Microbial community analyses

We determined abundances, biomass and composition of the microbial community in the initial hydrographic samples and experimental bottles with a combination of FCM, pigment analyses and microscopy (Selph *et al.*, 2021). Population abundances of *Prochlorococcus* (PRO), *Synechococcus* (SYN) and heterotrophic prokaryotes/bacteria (HBACT) were determined from 2-mL FCM samples, which were preserved with 0.5% paraformaldehyde (v/v), frozen in liquid nitrogen, and stored at −80°C until analysis. In the laboratory, the samples were thawed and stained with Hoechst 33342 (1 μg mL⁻¹, v/v) at room temperature in the dark for 1 h (Monger and Landry, 1993). Aliquots (100 μL) were analyzed with a Beckman–Coulter EPICS Altra flow cytometer with a Harvard Apparatus syringe pump for volumetric sample delivery. Simultaneous (co-linear) excitation was provided by two water-cooled 5-W argon ion lasers, tuned to 488 nm (1 W) and the UV range (200 mW). Calibration beads (0.5 and 1.0-μm yellow–green beads and 0.5-μm UV beads) were run in each sample as fluorescence standards, and FlowJo software was used to distinguish populations based on chlorophyll *a* (red fluorescence, 680 nm), phycoerythrin (orange fluorescence, 575 nm), DNA (blue fluorescence, 450 nm) and light-scatter signatures. Cell abundance estimates were converted to carbon biomass using factors of 11, 32 and 101 fg C cell⁻¹ for HBACT, PRO and SYN, respectively (Garrison *et al.*, 2000; Brown *et al.*, 2008).

Initial and final samples (250 mL) for fluorometric Chl*a* analyses were filtered onto GF/F filters and extracted with 90% acetone in a −20°C freezer for 24 h. Extracted samples were warmed to room temperature in the dark and analyzed on a Turner Designs model 10 fluorometer calibrated against a pure Chl*a* standard (Strickland and Parsons, 1972).

Concentrations of chlorophyll and carotenoid pigments were also determined using high-pressure liquid chromatography (HPLC) on 2.2-L samples filtered onto Whatman GF/F filters, frozen in liquid nitrogen and stored at −85°C. The samples were extracted and analyzed by the Horn Point Analytical Services Laboratory (HPL) at the University of Maryland Center for Environmental Science using a C8 column and a reversed phase, methanol-based solvent protocol and an automated 1100 HPLC system with temperature-controlled autosampler, Peltier temperature-controlled column oven compartment and PDA detector (Van Heukelem and Thomas, 2001; Hooker *et al.*, 2012).

Monovinyl and divinyl Chl*a* were detected at 665 nm. Carotenoids and xanthophylls were detected at 450 nm. Concentrations were quantified from chromatograms relative to run standards using Agilent ChemStation software.

Select samples in the upper two (mixed layer) and the lower two (DCM) sampling depths for the C1, C4 and C5 experiments were analyzed by microscopy to determine carbon concentrations for >2-μm protists and phytoplankton C:Chl*a* conversion factors for the upper and lower euphotic zone. Seawater samples (500 mL) for analysis by epifluorescence microscopy (EPI) were preserved with 260 μL of alkaline Lugol's solution, 10 mL 0.08 M borax-buffered 10% formalin and 500 μL 0.19 M sodium thiosulfate (Sherr and Sherr, 1993) and stained with 1 mL of proflavine (0.33% w/v) and 1 mL of DAPI (0.01 mg mL^{-1}) prior to filtering. Subsamples of 50 mL were filtered onto 25-mm, black, 0.8-μm pore polycarbonate filters to enumerate small cells at ×630 magnification. The remaining 450 mL was filtered onto 25-mm, black, 8.0-μm pore polycarbonate filters to count larger cells at ×200. Each filter was mounted onto a glass slide using Type DF immersion oil and a No. 2 cover slip.

The slides were imaged and digitized using an automated Zeiss Axiovert 200 M inverted epifluorescence microscope, with an AxioCam MRc black and white 8-bit CCD camera (Taylor et al., 2016). Fifty random positions were imaged for each slide, with each position consisting of four fluorescent channels: Chl*a*, DAPI (DNA stain), FITC (proflavin protein stain, cell outline) and phycoerythrin (PE). In addition, 6–7 Z-plane images were acquired at each position for each fluorescence channel. The resulting z-stack images were combined using an extended depth of field algorithm to produce one in-focus image for each position and channel (Chl*a*, DAPI, FITC and PE). These were then false colored (red, blue, green and orange, respectively) and combined into a single composite 24-bit RGB image for each position. Cell biovolumes (BV; μm³) were determined from length (L) and width (W) measurements according to Taylor et al. (Taylor et al., 2011) from images that passed quality inspection. Image processing and analysis was carried out in Image Pro software. Carbon (C; pg cell^{-1}) biomass was computed from BV from the equations: $C = 0.216 \times BV^{0.939}$ for non-diatoms and $C = 0.288 \times BV^{0.811}$ for diatoms (Menden-Deuer and Lessard, 2000).

Seawater samples (150 mL) were also preserved with 5% acid Lugol's solution for separate analyses of ciliates, concentrated onto 25-mm 8.0-μm polycarbonate membranes and prepared as slides according to the protocol of Freibott et al. (Freibott et al., 2014). The slides were imaged on a Zeiss AxioVert 200 M inverted microscope at ×200 magnification using brightfield illumination and processed using Image Pro software as described for EPI microscopy. Length and width measurements were used to calculate cell biovolumes (BV, μm³) based on the most appropriate cell shape, and carbon biomass was calculated as $pg\ C = 0.19 \times BV$ (Putt and Stoecker, 1989).

Growth, production and grazing rates

We determined rate profiles for phytoplankton growth (μ, day^{-1}) and microzooplankton grazing (m, day^{-1}) from each pair of dilution experiment bottles and for each FCM or pigment-associated population according to the following equations:

$$m = (k_d - k)/(1 - D) \text{ and } \mu = k + m$$

where k_d and k are the measured net rates of change between initial and final concentrations in the diluted and undiluted treatments, respectively, and D is the portion of unfiltered water in the dilution treatment (Landry et al., 2008; Selph et al., 2011). Rate estimates assume comparable growth rates in dilution treatments and proportional grazing relative to dilution, consistent with the expected close coupling of production, grazing and nutrient remineralization in the microbial communities of ultra-oligotrophic systems. Fluorometric Chl*a* samples were generally replicated in initial and final samples, and the rate estimates were based on mean fluorometer readings and acid ratios from initial and final treatments at each experimental depth. FCM population and HLPC pigment measurements were unreplicated for each bottle. Unless otherwise noted, we present experimental uncertainties as ±standard errors of mean estimates (±SEM), treating each day of each cycle as an independent experiment. Depth-averaged rate estimates were determined by integrating rate estimates from the surface to the deepest incubation depth according to the trapezoidal rule and dividing by depth.

Carbon-based estimates of phytoplankton community production (PROD) and microzooplankton grazing (GRAZ) were calculated from growth (μ) and grazing (m) rates for total Chl*a* from dilution experiments and the following equations (Landry et al., 2000):

$$PROD = \mu \times C_o \left(e^{(\mu-m)t} - 1 \right) / (\mu - m)\, t \text{ and}$$
$$GRAZ = m \times C_o \left(e^{(\mu-m)t} - 1 \right) / (\mu - m)\, t$$

where C_o is initial autotrophic biomass (mg C m^{-3}) and t is time (1 day). For estimates of community carbon at the middle experimental depths of each profile, we used the C:Chl*a* ratios of Selph et al. (Selph et al., 2021). Group-specific estimates of carbon production and

grazing were similarly calculated for populations where parameter estimates of μ and m could be reasonably associated with a C-based estimate of standing stock. For example, production and grazing rates for PRO, SYN and HBACT were derived from FCM dilution rates and FCM estimates of population C biomass. For eukaryotic phototrophs, we used rate estimates for group-associated pigments [fucoxanthin (FUCO) for diatoms (DIAT), peridinin (PER) for plastidic dinoflagellates (ADINO), 19′-hexanoyloxy fucoxanthin (HEX) for prymnesiophytes (PRYMN), 19′-butanoyloxy fucoxanthin (BUT) for pelagophytes (PELAGO), monovinyl Chl*b* (MVChl*b*) for chlorophytes (CHLORO)] and estimates of group-specific carbon values based on the modified CHEMTAX analysis of Selph *et al.* (Selph *et al.*, 2021). This approach distributes the total C biomass among taxa based on CHEMTAX distribution of Chl*a*, assuming a similar C:Chl*a* ratio for all taxa. Depth-integrated rates of PROD and GRAZ were determined by summing the rates in each depth stratum to the deepest depth of the experimental incubations according to the trapezoidal rule.

RESULTS

Environmental conditions

All experimental incubations in the GoM were done under environmental conditions that can be described as warm-water, stratified, oceanic and oligotrophic (Table I). The surface mixed-layer depth (MLD), defined by a density difference of 0.1 kg m^{-3} relative to 10 m, varied from 31.5 (C1) to 12.4 m (C5) and was characterized by mean temperatures of 24.5 (C1) to 26.7°C (C3), salinities of 35.6 (C5) to 36.6 psu (C2, C3), and low chlorophyll of 0.07 (C2) to 0.13 mg Chl*a* m^{-3} (C5). Nitrate concentrations, measured by the low-level method (Knapp *et al.*, this issue), never exceeded 0.042 μM in the mixed layer and ranged, on average, from 0.01 (C2) to 0.08 μM (C4) over the depth range of experimental sampling. Total inventories of nitrate and chlorophyll integrated over the experimental depth range (NO3$_Z$ and CHL$_Z$; Table I) were also indicative of the oligotrophic open ocean (1.6–9.4 mmol N m^{-2}; 13.7–29.2 mg Chl*a* m^{-2}). C5, located closest to the shelf break and Mississippi River outflow (Fig. 1), was the most different of the experimental cycles, with the lowest salinity, the highest Chl*a* and the shallowest DCM (78 m vs 100–137 m for C1–C4). It did not, however, have a higher NO3$_Z$ inventory than the average of 5.7 ± 1.4 mmol N m^{-2} for all cycles. As observed by Selph *et al.* (Selph *et al.*, 2021), T–S relationships in the upper 100–150 m remained coherent throughout the C1–C4 experiments, indicating the drift

array remained within the initial waters. For C5, however, which began close to the edge of the Florida Escarpment in the northeastern gulf, the initial waters showed a fresh-water influence and mixed with saltier offshore waters during transport.

Two trends were noted in the repeated daily sampling following the experimental drift array (Fig. 2). First, all experiments were conducted during periods of euphotic zone warming. The mixed layer exhibited the strongest rate of temperature increase, ranging from 0.09 (C4) to 0.21°C day^{-1} (C5) and averaging 0.14 ± 0.05°C day^{-1} overall (Fig. 2A). Mean temperatures of the water column to a fixed depth of 100 m (T$_{100m}$ in Table I) also increased during each cycle at a mean rate of 0.08 ± 0.02°C day^{-1}. Second, Chl*a* concentrations were not at steady state during any of the cycles. Depth-integrated Chl*a* inventories (CHL$_Z$) decreased during C2 and C3 at mean rates of -1.9 and -0.8 mg Chl*a* m^{-2} day^{-1}, respectively. By contrast, during C1, C4 and C5, CHL$_Z$ increased at mean rates of 1.2, 1.3 and 6.7 mg Chl*a* m^{-2} day^{-1}, respectively. Mean mixed-layer concentrations of Chl*a* (CHL$_{ML}$) did not, however, show a significant trend during any cycle, varying from rates of -0.027 to $+0.006$ mg Chl*a* m^{-3} day^{-1} and averaging -0.007 ± 0.008 mg Chl*a* m^{-3} day^{-1} for all cycles. Thus, temporal changes in CHL$_Z$ during the drift experiments mainly reflected net rates of growth, loss or advective flow in the water column below the mixed layer and above the DCM.

Phytoplankton community rates of growth and grazing mortality

Community-level rates of phytoplankton growth and microzooplankton grazing mortality are derived from fluorometric and HPLC measurements of Chl*a*, which we distinguish as FlChl*a* and TChl*a*, respectively. We illustrate the general features and variability of individual rate profiles based on FlChl*a* in Fig. 3 and compare mean cycle profiles for the two Chl*a* measurements in Fig. 4.

Individual rate profiles from FlChl*a* typically show peak, or close to maximum, growth rates of 0.6 to 1.0 day^{-1} in the mid-euphotic zone (Fig. 3). C4 is the clearest example of this, with relatively low variability among rate profiles and highest growth rate at 60 m on 3 of the 4 days. Occasional anomalous estimates are also evident in the profiles, such as the much higher growth rate (~ 1.5 day^{-1}) at 20 m on C1.2 (Cycle 1, day 2) and a negative estimate (-0.15 day^{-1}) at 25 m on C5.4. While neither of these estimates are anomalous in TChl*a* profiles (not shown), the latter have unexplained variability on other days and depths. In subsequent figures, such measurement variability is incorporated into the error bars in mean cycle profiles. Individual profiles for grazing rates occasionally

Table I: Environmental conditions for experimental cycles in the Gulf of Mexico during May 2017 (Cycles 1–3) and May 2018 (Cycles 4–5)

Variable	Cycle 1	Cycle 2	Cycle 3	Cycle 4	Cycle 5
Dates	11–14 May	16–18 May	27–30 May	5–9 May	15–19 May
Profiles (n)	4	3	4	5	5
MLD (m)	31.5 ± 4.0	24.2 ± 1.1	25.8 ± 4.1	23.7 ± 1.2	12.4 ± 0.5
DCM (m)	100 ± 1.3	120 ± 7.9	137 ± 1.7	111 ± 7.1	78 ± 3.9
EZ (m)	100 ± 0.0	n.d.	126 ± 2.4	99 ± 8.8	87 ± 3.6
T_{ML} (°C)	24.5 ± 0.12	25.3 ± 0.06	26.7 ± 0.07	25.6 ± 0.07	25.5 ± 0.14
T_{100m} (°C)	23.4 ± 0.06	24.6 ± 0.05	25.4 ± 0.04	24.8 ± 0.04	23.5 ± 0.12
S_{ML} (psu)	36.41 ± 0.009	36.57 ± 0.004	36.55 ± 0.002	36.42 ± 0.012	35.64 ± 0.14
$NO3_{AVG}$ (µM)	0.05 ± 0.01	0.01 ± 0.01	ND	0.08 ± 0.04	0.06 ± 0.02
$NO3_Z$ (mmol m^{-2})	5.0 ± 1.5	1.6 ± 0.8	ND	9.4 ± 4.3	4.4 ± 1.2
CHL_{ML} (mg m^{-3})	0.08 ± 0.01	0.07 ± 0.02	0.09 ± 0.01	0.10 ± 0.01	0.13 ± 0.01
CHL_Z (mg m^{-2})	17.7 ± 1.0	16.2 ± 1.4	13.7 ± 0.7	24.1 ± 1.2	29.2 ± 5.4

MLD (m) = mixed-layer depth, defined as the depth at which seawater density is 0.1 kg m^{-3} greater than at 10 m. DCM (m) = depth of the deep chlorophyll maximum; EZ (m) = depth of the euphotic zone (1% surface PAR); T_{ML} (°C) = mean temperature of the mixed layer; T_{100m} (°C) = mean temperature of the upper 100 m; S_{ML} (psu) = mean salinity of the mixed layer; and $NO3_{AVG}$ (µM) and $NO3_Z$ (mmol m^{-2}) are mean concentrations and depth-integrated concentrations of NO$_3$ to the depth of experimental incubations. CHL_{ML} (mg m^{-3}) and CHL_Z (mg m^{-2}) are the average mixed-layer concentrations and depth-integrated concentrations to the depth of experimental incubations for fluorometrically measured Chl$a$. Uncertainties are standard errors of mean values.
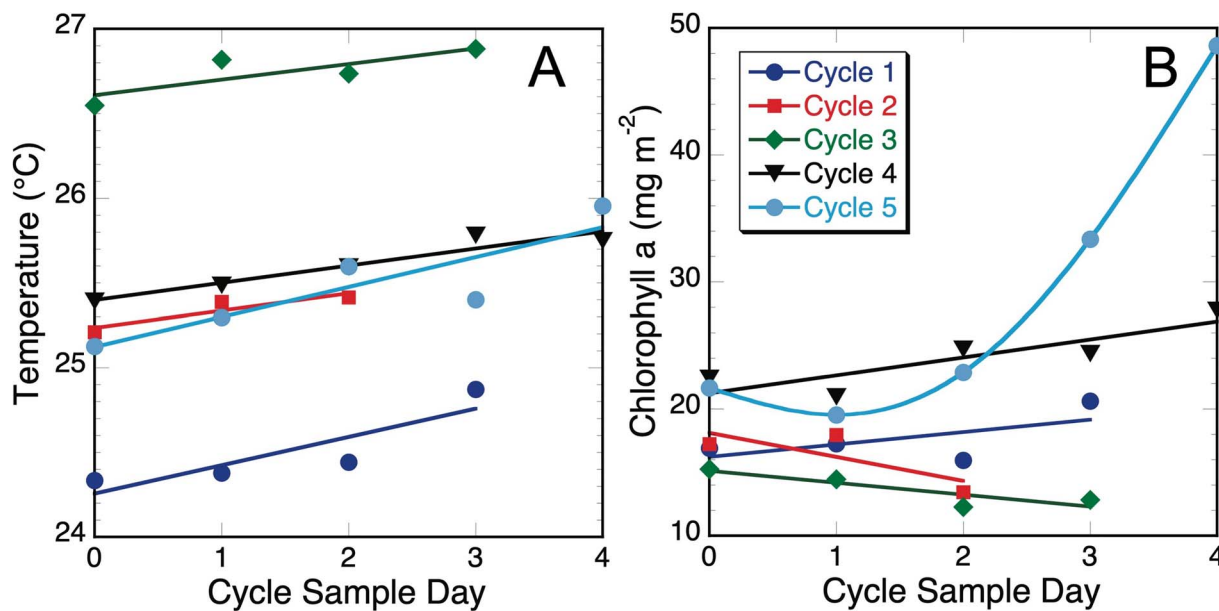

Fig. 2. Daily values of mixed-layer temperature (**A**) and depth-integrated chlorophyll a (**B**) during Cycles 1–5 drift experiments in the Gulf of Mexico.

parallel the contemporaneous profiles for growth rates, but not proportionately and with subtle-to-substantial differences.

Comparisons of mean growth and grazing rate profiles from FlChl$a$ and TChl$a$ reveal some differences (Fig. 4). Profiles for C4 are the most similar with respect to magnitudes and depth distributions, with both showing growth and grazing peaks in the mid-euphotic zone (40–60 m). The patterns diverge for C1 and C5, especially with respect to near-surface grazing, which tend to be maximum values in TChl$a$ profiles but local grazing minima in FlChl$a$ profiles. Overall, FlChl$a$ and TChl$a$

rate estimates are significantly correlated ($P < 0.001$), but a low portion of the variability is explained ($r^2 = 0.29$ for growth; 0.30 for grazing). Since FlChl$a$ concentrations were 2-fold higher, on average, than HPLC values in our samples, the rate profile differences suggest that the fluorescence contributions of other pigments (e.g. chlorophyllide, Chl$b$) were different enough from true Chl$a$ to affect the mean rate profiles. As to commonalities, the FlChl$a$ and TChl$a$ profiles both show reduced rates of phytoplankton growth, on average, in near-surface waters. Using bead-normalized red fluorescence to evaluate changes in cellular Chl$a$ content of

FCM-measured populations between initial and final incubation samples (e.g. Landry *et al.*, 2011b), we could not explain these low growth estimates as photo-bleaching or cellular photo-acclimation effects. Both sets of profiles also indicate that phytoplankton growth and microzooplankton grazing mortality are more closely balanced, on average, in near-surface waters and the DCM, leaving broad depth intervals in the intermediate euphotic zone where phytoplankton growth more clearly exceeds grazing (Fig. 4).

Population-specific rates of growth and grazing mortality

FCM populations generally show relatively high rates of growth and grazing in the upper 20 m, often with grazing estimates close to or exceeding growth in near-surface (5 m) waters (Fig. 5). Maximum growth rate estimates of photosynthetic bacteria (PRO and SYN) are higher (0.6–0.9 day^{-1}) for C4 and C5 compared to C1 (0.4–0.5 day^{-1}). HBACT growth rates are more similar for C1 and C4 (0.2–0.3 day^{-1}), but elevated (0.4–0.5 day^{-1}) for C5. Significant growth rates also extend to the DCM for all populations, particularly for deep-living SYN. Grazing estimates closely parallel growth rate profiles with relatively modest differences in mean rates for C4 and C5. For C1, however, there are more substantial differences between growth and grazing estimates between surface waters and the DCM.

Rate estimates from the accessory pigments FUCO, PER and hex-fucoxanthin (HEX) are taken to be indicative of growth and grazing of DIAT, autotrophic dinoflagellates (ADINO) and PRYMN, respectively (Fig. 6). In contrast to photosynthetic bacteria (Fig. 5), maximum growth rates of these eukaryotic taxa are higher for C1 (~0.8–1.1 day^{-1}) than C5 (0.4–0.8 day^{-1}). Maximum growth estimates (1.1–1.3 day^{-1}) are highest for C4, with FUCO and HEX exhibiting strong subsurface peaks at 55 m while high growth for PER extends broadly over the upper 40 m. As in mean rate profiles for Chl*a* and FCM populations, grazing rates are comparable to and often exceed growth rate estimates for experiments with near-surface and DCM water, though FUCO results for C1 are exceptional in showing a wide discrepancy between growth and grazing of DIAT throughout the profile compared to PER and HEX (Fig. 6).

Carbon-based estimates of production and grazing

The carbon-based rate estimates for production (PROD) and grazing (GRAZ) in Table II were calculated from biomass measurements and instantaneous rates for individual experiments and then integrated for daily profiles and averaged for each cycle. For Cycles 1, 4 and 5, three estimates of community rates can be compared—from FlChl*a* and TChl*a* rates and total autotrophic carbon and from the sum of the computed rates for individual populations. Community PROD estimates range from 415 to 465 mg C m^{-2} day^{-1} for C1, from 322 to 431 mg C m^{-2} day^{-1} for C4 and from 234 to 333 mg C m^{-2} day^{-1} for C5. Community GRAZ estimates range from 248 to 366 mg C m^{-2} day^{-1} for C1, 189 to 278 mg C m^{-2} day^{-1} for C4 and 172 to 207 mg C m^{-2} day^{-1} for C5. In pair-wise *t*-tests, overall results from the different approaches were not significantly different from one another for either PROD ($P > 0.06$) or GRAZ ($P > 0.13$). Integrated PROD and GRAZ rates decline progressively from C1 to C5, but the rate differences between years (*t*-test, $P > 0.49$) or between C1 and C5 ($P > 0.16$) are not significant. Overall rate averages of 358 ± 27 mg C m^{-2} day^{-1} for PROD and 233 ± 22 mg C m^{-2} day^{-1} for GRAZ therefore reasonably describe results for the three major cycles. On average, $66 \pm 5\%$ of phytoplankton production is consumed by microzooplankton grazers. For the combined C2–C3 experiments, the available rates for FlChl*a* and FCM bacterial populations are relatively low compared to the other cycles, considering that they were integrated over deeper euphotic zones (Table I). It thus appears that environmental conditions were particularly oligotrophic for C2–C3, during which water-column Chl*a* was observed to decline (Fig. 2).

Estimates of HBACT production based on FCM cell counts and dilution rates are higher for the 2018 cruise (C4–5; 183 ± 26 mg C m^{-2} day^{-1}) compared to 2017 (C1–3; 78 ± 11 mg C m^{-2} day^{-1}) ($P < 0.003$) and are also a higher percentage of phytoplankton PROD based on FlChl*a* ($49 \pm 10\%$ vs $21 \pm 3\%$; $P < 0.024$; Table II). Microzooplankton grazing rates on HBACT are similarly higher in 2018 experiments (154 ± 25 vs 45 ± 6 mg C m^{-2} day^{-1}; $P < 0.003$) but not significantly higher in terms of % HBACT production consumed ($83 \pm 6\%$ vs $63 \pm 9\%$; $P > 0.08$).

Despite the similarities noted above in mean rates for the total community for cycle experiments, substantial differences are evident between years in the relative contributions of populations to phytoplankton PROD and GRAZ (Table II). For PRO, mean PROD (174 ± 16 vs 132 ± 10 mg C m^{-2} day^{-1}; $P < 0.043$) and GRAZ (110 ± 9 vs 74 ± 12 mg C m^{-2} day^{-1}; $P < 0.032$) are significantly higher for 2018 than 2017, but the percentages of PRO production grazed ($64 \pm 5\%$ vs $55 \pm 7\%$; $P > 0.32$) are similar. For SYN, estimates of PROD (55 ± 4 vs 18 ± 2 mg C m^{-2} day^{-1}; $P < 0.0001$), GRAZ (46 ± 5 vs 6 ± 2 mg C m^{-2} day^{-1}; $P < 0.0001$) and
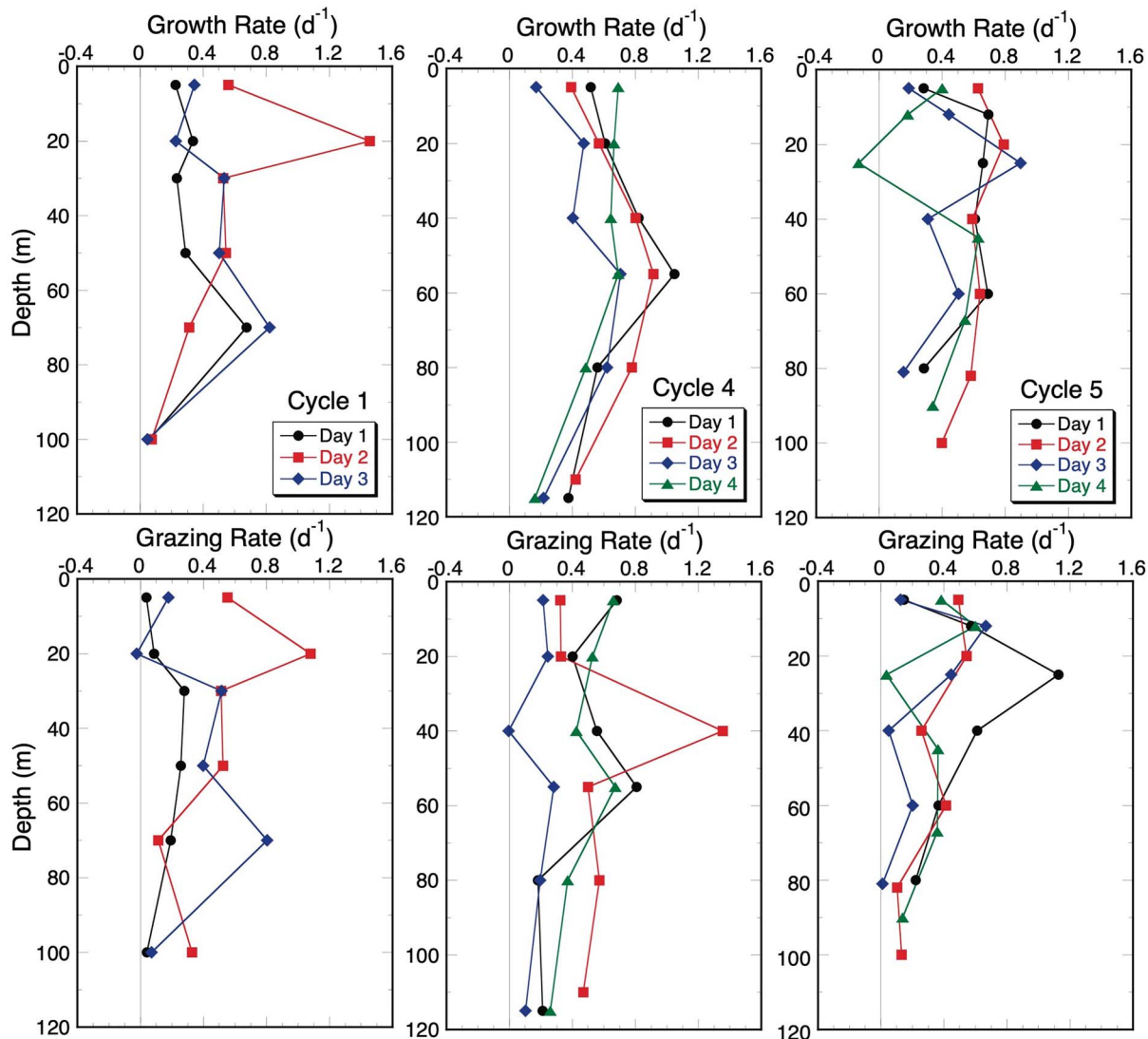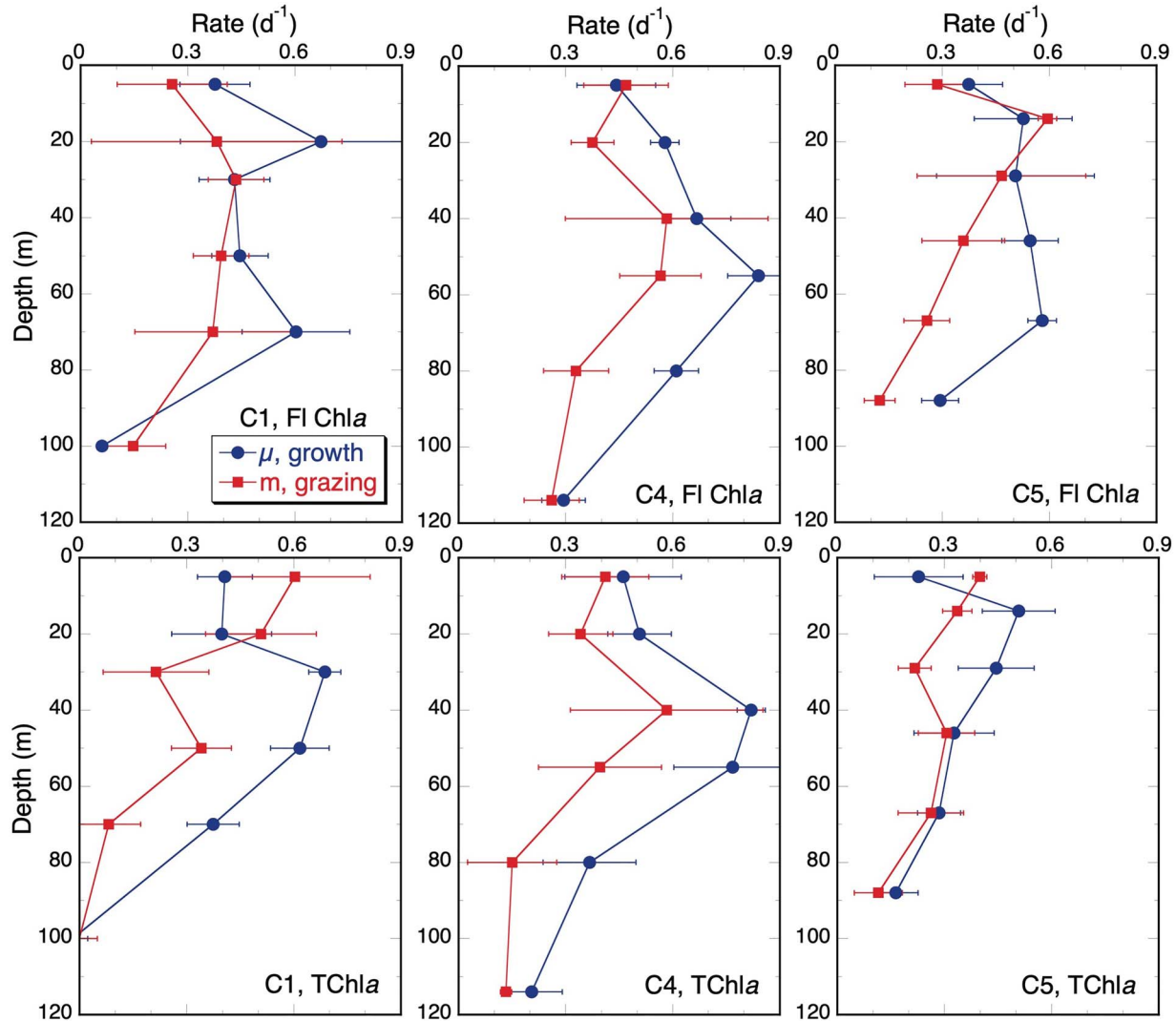
Fig. 3. Daily rate profiles for phytoplankton growth and microzooplankton grazing based on fluorometric Chl*a* during Cycles 1, 4 and 5 drifter experiments in the Gulf of Mexico.

% production grazed ($82 \pm 6\%$ vs $30 \pm 7\%$; $P < 0.0001$) are all higher in 2018 than 2017. Rates for eukaryotic taxa are higher on average in 2017, but the differences are not statistically significant. For example, due to only three experiments in 2017, the cruise production differences for PRYMN give a P value > 0.26. Nonetheless, PRYMN and PRO are co-dominant contributors to phytoplankton community PROD and GRAZ for C1 (2017), while PRO is the clear dominant taxa for C4–5 (2018) (Fig. 7). Diatoms and dinoflagellates are notably small contributors to community PROD and GRAZ, despite having high instantaneous rates of growth and grazing throughout the euphotic zone (Fig. 6).

Carbon-specific grazing by microzooplankton

Carbon-specific estimates of microzooplankton grazing are computed in Table III from the combined grazing on phytoplankton (FlChl*a*) and HBACT in Table II and microscopical estimates of heterotroph carbon. Most of the biomass resides in Other Heterotrophs, unrecognizable as specific taxa, and almost all (98%) is in cells <10 µm. Heterotrophic dinoflagellates and ciliates are smaller components of the total but comprise 66% of the biomass in cells ≥ 10 µm. We also consider that some of the phytoplankton may function as mixotrophs and assign to that group all of the biomass associated with ADINO

Fig. 4. Mean rate profiles of phytoplankton growth and microzooplankton grazing based on fluorometric Chl*a* and HPLC TChl*a* during Cycles 1, 4 and 5 drifter experiments in the Gulf of Mexico. Uncertainties are standard errors of mean estimates.

and 50% of the biomass of PRYMN. The latter is a somewhat arbitrary percentage but assumes that much of the biomass of PRYMN, PELAGO, CHLORO and PRAS is likely to reside in pico-sized cells that can compete with photosynthetic bacteria for dissolved nutrients and possibly lack the volume capacity or functionality for phagotrophy. In experimental studies in the equatorial Pacific, pigmented nanoflagellates were also observed to take up fluorescently labeled bacteria at half of the biomass-specific rates as non-pigmented flagellates (Stukel *et al.*, 2011).

Based on the estimates of total community grazing impact, if grazing is done by heterotrophic protists only, their consumption averages 78, 133 and 158% of body C day^{-1} for C1, C4 and C5, respectively

(Table III). If the biomass of presumptive mixotrophs also contributes to grazing, C-specific grazing estimates decrease to 61, 116 and 126% of body C day^{-1}. These are minimal estimates that do not consider nutritional resources, such as intra-guild predation (consumption of smaller grazers by larger microzooplankton), consumption of non-living (detrital) resources or nutritional contributions from phototrophy, kleptoplasty or endosymbionts. Assuming heterotrophic protists are the only grazers and have growth efficiencies of 30% (Straile, 1997; Landry *et al.*, 2020), instantaneous growth rates of the grazers can be calculated from the daily growth increment of 0.3× total grazing relative to the carbon biomass of heterotrophs
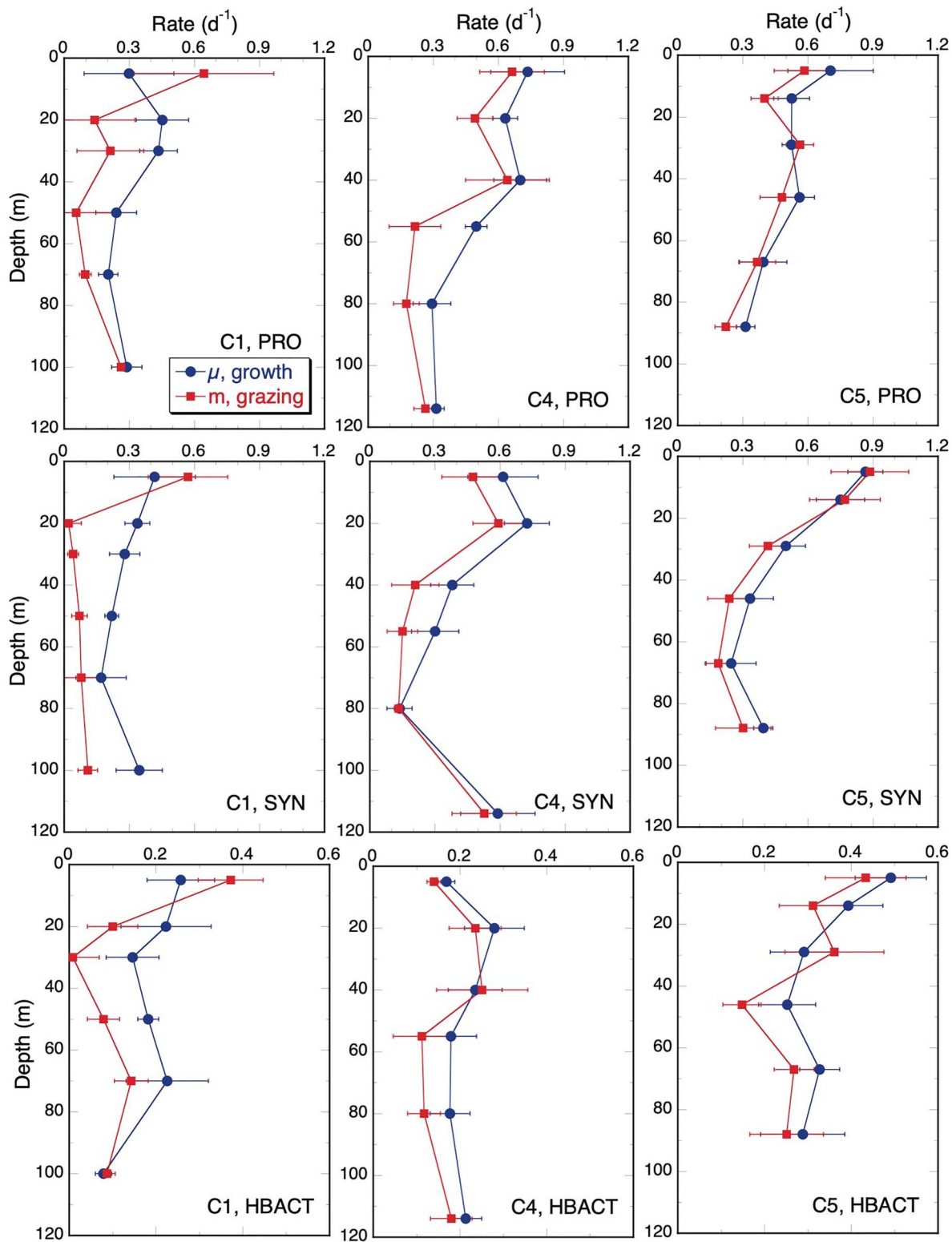
Fig. 5. Mean rate profiles of growth and grazing for flow cytometry populations during Cycles 1, 4 and 5 drifter experiments in the Gulf of Mexico. PRO = *Prochlorococcus*; SYN = *Synechococcus*; HBACT = heterotrophic bacteria. Uncertainties are standard errors of mean estimates.
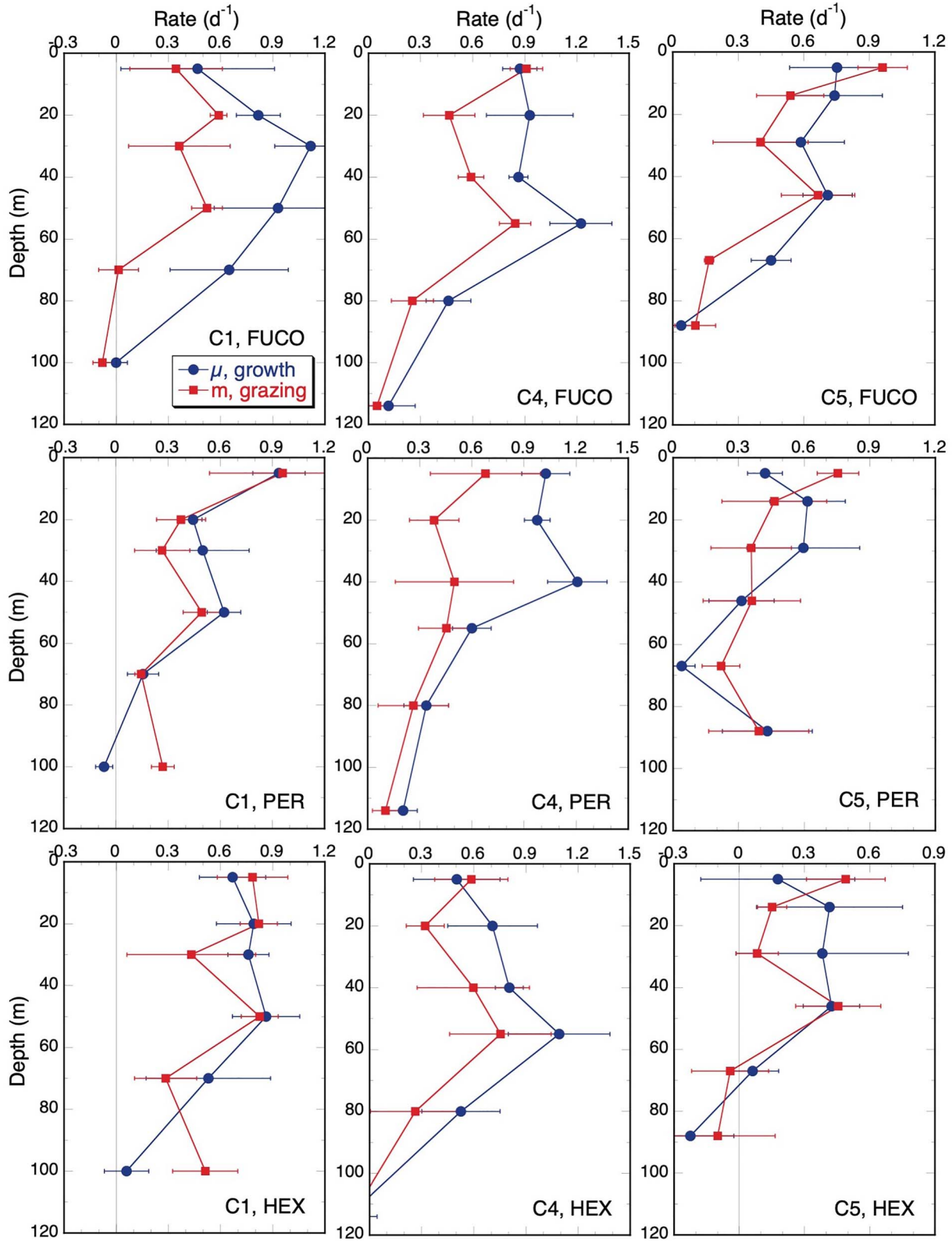
Fig. 6. Mean rate profiles of growth and grazing based on HPLC-measured pigments fucoxanthin (FUCO), peridinin (PER) and hex-fucoxanthin (HEX) during Cycles 1, 4 and 5 drifter experiments in the Gulf of Mexico. Uncertainties are standard errors of mean estimates.

Table II: Community and group-specific estimates of phytoplankton production and grazing in the Gulf of Mexico

Measurement	Cycle 1		Cycles 2–3		Cycle 4		Cycle 5	
	PROD	GRAZ	PROD	GRAZ	PROD	GRAZ	PROD	GRAZ
FlChl*a*	465 ± 66	366 ± 109	360 ± 70	225 ± 43	431 ± 33	278 ± 42	333 ± 28	207 ± 17
TChl*a*	455 ± 100	248 ± 82			374 ± 48	200 ± 61	234 ± 22	172 ± 28
NPP (H^{13}CO$_3^-$)	308 ± 1		296 ± 14		344 ± 38		351 ± 30	
HBACT_fcm	87 ± 23	55 ± 9.0	83 ± 13	43 ± 4.8	137 ± 25	110 ± 20	229 ± 33	197 ± 34
Phytoplankton groups								
PRO_fcm	152.0 ± 17	88.1 ± 28	113.0 ± 12	63.9 ± 13	204.0 ± 19	118.0 ± 15	145.0 ± 13	102.0 ± 12
SYN_fcm	21.7 ± 2.3	9.8 ± 1.7	18.0 ± 0.9	4.9 ± 1.3	50.6 ± 5.0	36.0 ± 5.4	60.4 ± 6.0	55.3 ± 6.2
PRYMN_HEX	134.0 ± 59	126.0 ± 28			82.5 ± 16	43.1 ± 22	33.5 ± 4.0	26.9 ± 3.3
PELAGO_BUT	27.3 ± 14	11.9 ± 4.7			3.6 ± 1.9	2.2 ± 0.6	4.5 ± 3.0	3.1 ± 0.9
ADINO_PER	12.6 ± 5.3	11.6 ± 3.6			6.1 ± 1.5	2.7 ± 0.7	3.7 ± 1.1	4.3 ± 0.9
DIATOM_FUCO	10.2 ± 4.5	4.8 ± 2.1			2.3 ± 1.0	1.5 ± 0.6	1.7 ± 0.4	2.0 ± 0.6
CHLORO_MVChl*b*	46.8 ± 16	23.8 ± 12			2.3 ± 1.6	2.0 ± 1.1	6.7 ± 2.0	7.9 ± 2.0
PRAS_PRASIN	11.6 ± 2.2	4.9 ± 1.6			0.4 ± 0.3	0.0 ± 0.0	5.5 ± 4.7	8.7 ± 8.1
Total	415 ± 95	280 ± 76			322 ± 23	189 ± 18	255 ± 22	202 ± 14

Community total rates are based on full phytoplankton carbon and instantaneous growth and grazing rates from fluorometric (FlChl*a*) and HPLC (TChl*a*) and Net Primary Production (NPP) from uptake of ^{13}C-labeled bicarbonate. All other rates are based on relevant components of phytoplankton carbon and instantaneous rates from flow cytometry (fcm) or HPLC pigments (PER = peridinin; HEX = hex-fucoxanthin; BUT = butfucoxanthin; FUCO = fucoxanthin; PRASIN = prasinoxanthin). PRO = *Prochlorococcus*; SYN = *Synechococcus*; HBACT = heterotrophic bacteria, PRYMN = prymnesiophyte; PELAGO = pelagophyte; ADINO = autotrophic dinoflagellate; CHLORO = chlorophyte; PRAS = prasinophyte. All rates are mg C m^{-2} day^{-1}. Uncertainties are standard errors of mean values.
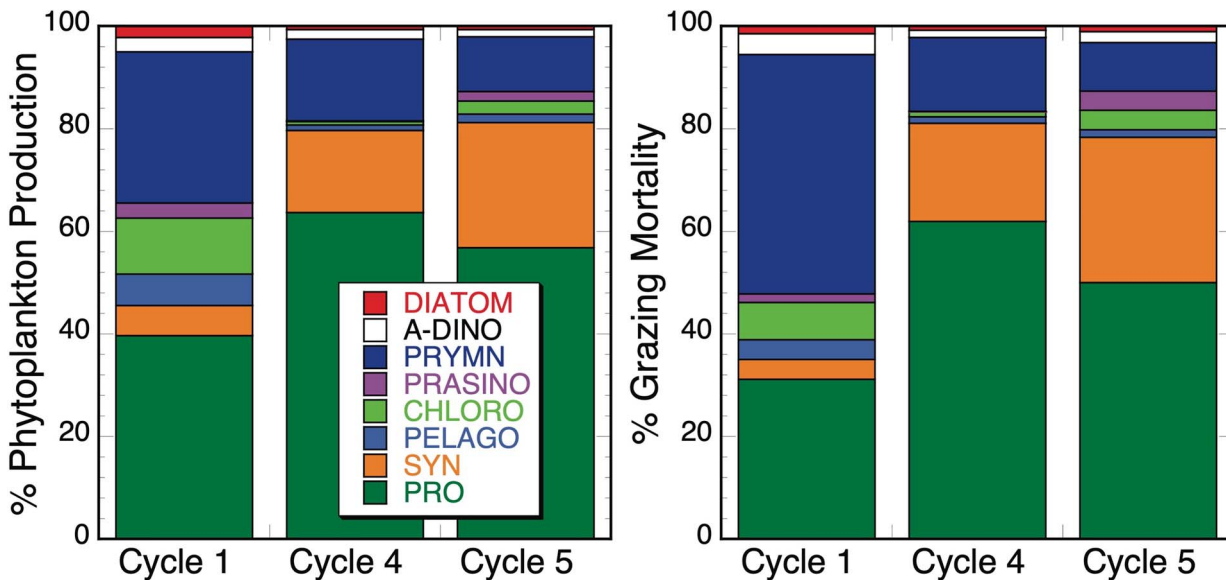

Fig. 7. Group-specific contributions to phytoplankton production and microzooplankton grazing during Cycles 1, 4 and 5 drift experiments in the Gulf of Mexico. A-DINO = autotrophic dinoflagellate; PRYMN = prymnesiophyte; PRASINO = prasinophyte; CHLORO = chlorophyte; PELAGO = pelagophyte; PRO = *Prochlorococcus*; SYN = *Synechococcus*.

in Table III, yielding estimates of 0.21 (C1), 0.34 (C4) and 0.39 day^{-1} (C5). The higher 2018 estimates would allow heterotrophic protists to grow at rates comparable to the water-column averages for pigmented cells (e.g. 0.31–0.50 day^{-1} based on FlChl*a* and TChl*a*). For C1, the implied growth rates of heterotroph grazer biomass, without consideration of sharing ingestion with mixotrophs, falls short of the water-column average for pigmented cells (0.36–0.38 day^{-1}).

Table III: Calculations of microzooplankton grazing as % body carbon day⁻¹ for experimental cycles in the Gulf of Mexico

Variable	Cycle 1	Cycle 4	Cycle 5
Total Grazing (mg C m^{-2} day^{-1})	421 ± 117	388 ± 32	404 ± 35
Carbon Biomass (mg C m^{-2})			
Ciliate	68 ± 15	80 ± 5	57 ± 1
HDino	21 ± 8	17 ± 2	14 ± 2
Other	442 ± 86	200 ± 30	255 ± 67
Total Heterotroph	530 ± 107	297 ± 26	326 ± 70
Mixotroph	141 ± 30	44 ± 10	82 ± 22
Total Hetero + Mixo	671 ± 136	341 ± 25	408 ± 90
Percent Body Carbon Consumed (%C day^{-1})			
Heterotroph	78 ± 15	133 ± 14	158 ± 55
Hetero + Mixo	61 ± 11	116 ± 14	126 ± 41

Total Grazing (mg C m^{-2} day^{-1}) is the sum of grazing estimates on phytoplankton (Chl*a*_fluor) and HBACT from Table II. Carbon Biomass (mg C m^{-2}) estimates are from microscopical analyses of EPI slides (H-Dino and Others) and acid Lugols preserved samples (Ciliates). Biomass of presumptive mixotrophs includes all ADino and 50% of PRYMN from Selph *et al.* (Selph *et al.*, 2021). Uncertainties are standard errors of mean values.

DISCUSSION

Daily incubation profiles incorporate measurement uncertainties in the initial and final samples used to compute growth and grazing rates in the individual experiments at each depth, as well as uncertainties in the assessments of community and population biomasses. They consequently give variable rate relationships for the microbial community on a given day rather than high-precision results. Nonetheless, repeated daily profiles along the drift path and rate estimates from a variety of measured parameters allow some conclusions to be made about the magnitudes of phytoplankton and bacterial production, differences in contributions of dominant taxa between the two cruise years, grazing impacts relative to production rates and grazer biomass, and the depth range of the euphotic zone where net phytoplankton growth generally occurs. In the discussion sections below, we first put the present results in the context of previous studies of other regions with similar methods. We then consider how these different findings contribute to a better understanding of microbial community dynamics in the open-ocean Gulf of Mexico, as well as some of the issues that they raise.

Regional comparisons

Relatively few studies have resolved group-specific contributions to community-level production and grazing, but some oceanic areas have sufficient data by similar methods to compare to the GoM, including open-ocean upwelling regions of the equatorial Pacific (Landry *et al.*, 2011a), Costa Rica Dome (Landry *et al.*, 2016a, b) and the subtropical Pacific studied in (OPAL) and out (Ambient) of an Hawaiian lee eddy with a massive subsurface diatom bloom (Landry *et al.*, 2008). Because euphotic zone depths vary inversely with phytoplankton concentrations, the systems tend to be relatively similar in terms of integrated Chl*a* and phytoplankton C, yet group contributions to production and grazing are very different (Table IV). For example, PRO typically dominates among photosynthetic bacteria and comprises a large component of total community production, but SYN assumes that dominant role in the Costa Rica Dome (CRD). DIAT and ADINO are typically small contributors to community production, but both are equal or more important than PRO in the equatorial upwelling region. We cannot adequately compare the relative contributions of PRYMN among systems because it was not assessed in the subtropical experiments and PRYMN biomass was likely underestimated in microscopical analyses for the equatorial Pacific and CRD. In the present investigation, recognizable PRYMN biomass from epifluorescence microscopy underestimated biomass estimates from CHEMTAX (Selph *et al.*, 2021) by more than an order of magnitude, which greatly outweighs the uncertainties in C:pigment ratios. Conservatively, however, PRYMN contributions to production and grazing in the equatorial Pacific and CRD are at least of similar magnitude to determinations for the 2018 GoM experiments, though unlikely to be as high as the 2017 C1 experiments based on relative HEX pigment concentrations in these studies.

In general, estimates of primary production from dilution rates and carbon biomass agree reasonably with rates from standard H^{14}CO$_3^-$ or H^{13}CO$_3^-$ uptake experiments (Table IV). The latter are not available from contemporaneous measurements in the subtropical Pacific during the OPAL eddy study, but the three dilution profiles in ambient (non-eddy) waters do not differ significantly from the mean (±SD) values for integrated TChl*a* (26.8 ± 4.5 mg m^{-2}) and ^{14}C-based primary production (516 ± 53 mg C m^{-2} day^{-1}) from long-term study at Stn. ALOHA (Valencia *et al.*, 2018). Dilution production estimates should exceed rates from 24-h isotopic incubations by an amount that accounts for loss of fixed carbon to nocturnal respiration (Landry *et al.*, 2011a; Kranz *et al.*, 2020). The production estimates based on FlChl*a* (481 ± 59 and 404 ± 27 mg C m^{-2} day^{-1} for 2017 and 2018, respectively) fit this expectation better than TChl*a* values, which are notably low for C5. The GoM ratios of production to integrated TChl*a* [26 and 32 mg C (mg Chl*a*)$^{-1}$ day^{-1} for 2017 and 2018, respectively] are higher than the Stn. ALOHA average [19 mg C (mg Chl*a*)$^{-1}$ day^{-1}], although the latter is reduced by deeper

Table IV: Comparison of standing stocks, production and grazing rates estimated by similar methods in open-ocean ecosystems of the equatorial Pacific, Costa Rica Dome, Subtropical Pacific and Gulf of Mexico

Variable	Equatorial Pacific[a]	Costa Rica Dome[b]	Subtropical Pacific[c]		Gulf of Mexico[d,e,f]	
			Ambient	OPAL	2017	2018
Profiles	31	13	3	3	3 (8)	8
Intgr TChl$a$	26.7 ± 0.7	24.1 ± 1.5	26.2 ± 0.4	29.0 ± 2.9	11.8 ± 0.3	10.6 ± 0.7
Intgr Phyto C	1385 ± 47	1378 ± 112	1295 ± 145	2410 ± 82	1097 ± 73	701 ± 52
Production (mg C m^{-2} day^{-1})						
^{14}C Prim Prod	672 ± 37	1025 ± 113			308 ± 1	348 ± 37
TChl	867 ± 49	990 ± 106	550 ± 91	1538 ± 109	455 ± 100	304 ± 36
PRO	132 ± 11	58 ± 14	300 ± 86	266 ± 29	152 ± 17	174 ± 16
SYN	50 ± 4	190 ± 29	12 ± 1	7 ± 1	22 ± 2	55 ± 4
DIATOM	156 ± 28	31 ± 10	25 ± 16	783 ± 160	10 ± 1	2 ± 0.5
ADINO	272 ± 36				13 ± 1	5 ± 1
PRYMN	69 ± 8	60 ± 13			134 ± 4	40 ± 11
Grazing (mg C m^{-2} day^{-1})						
TChl Total	608 ± 40	645 ± 62	324 ± 59	805 ± 243	248 ± 82	186 ± 31
PRO	143 ± 12	54 ± 11	188 ± 50	129 ± 14	88 ± 28	110 ± 9
SYN	58 ± 6	236 ± 39	7 ± 1	5 ± 2	10 ± 2	46 ± 5
DIATOM	83 ± 14	5 ± 2	19 ± 14	480 ± 138	5 ± 2	2 ± 0.4
ADINO	167 ± 20				12 ± 4	3 ± 1
PRYMN	35 ± 5	34 ± 8			126 ± 2	23 ± 4

Parentheses indicate number of profiles for flow cytometric rate estimates if different from other rates. TChl$a$ from HPLC analyses and phytoplankton carbon are integrated values (mg m^{-2}) to the base of the euphotic zone. Primary production was measured by ^{13}C stable isotopes in the Gulf of Mexico (Yingling *et al.*, 2021). PRO = *Prochlorococcus*; SYN = *Synechococcus*; ADINO = autotrophic dinoflagellate; PRYMN = prymnesiophyte. All rates are mg C m^{-2} day^{-1}. Uncertainties are standard errors of mean values.
[a] Landry *et al.* (2011a).
[b] Landry *et al.* (2016b), Selph *et al.* (2016).
[c] Landry *et al.* (2008).
[d] This study.
[e] Selph *et al.* (2021).
[f] Yingling *et al.* (2021).

integration to the 0.1% light level at ∼175 m, where the ratio of C uptake to Chl$a$ is low. The C-specific rate of primary production for the GoM [0.28 and 0.50 mg C (mg C)$^{-1}$ day^{-1} for 2017 and 2018, respectively] are also comparable to the subtropical Pacific [0.48 mg C (mg C)$^{-1}$ day^{-1}] based on mean daily primary production and integrated phytoplankton carbon (1072 $\pm$ 18 mg C m^{-2}; Pasulka *et al.*, 2013) at Stn. ALOHA. Overall, phytoplankton production and grazing estimates from dilution experiments in the GoM are low compared to previously studied open-ocean systems, but they vary largely in proportion to measured differences in phytoplankton biomass and contemporaneous primary production.

Role of mixotrophs

Various studies have indicated that mixotrophy is pervasive in biomes of the Atlantic Ocean (Unrein *et al.*, 2007; Zubkov and Tarran, 2008; Hartmann *et al.*, 2012), notably involving small (<5 μm) flagellates that feed on bacteria. If mixotrophs in the GoM account for a similar portion of bacterivory as these studies suggest (∼70%, range 60–77%; Hartmann *et al.*, 2012), and if phototrophic bacteria are equally vulnerable to such grazers as HBACT, the potential carbon flows to

mixotrophic nanoflagellates from phagotrophy for C1, C4 and C5 would be 107, 185 and 248 mg C m^{-2} day^{-1}, respectively (Table II). These rates are equivalent to 25, 48 and 61% of the total grazing impact of microzooplankton for the same cycles (Table III). For C1, the bacterivory ascribed to mixotrophs by this calculation is reasonably close to our estimate (21%) for the contribution of presumptive mixotrophs to total biomass of protistan grazers (Table III), implying a more-or-less biomass-proportional contribution of mixotrophs to grazing. By contrast, our estimates of mixotroph grazing percentages for C4 and C5 are 3–4 times higher than the contributions of presumptive mixotrophs to grazer biomass (13 and 20%, respectively; Table III) and thus seem unlikely. It is possible, of course, that some of the biomass ascribed to heterotrophs may have been functionally mixotrophic, with very dim chloroplasts or utilizing the plastids from prey for photosynthesis. On the other hand, C4 and C5 are also the experiments in which the grazing attributed to heterotrophs is sufficient for heterotroph protists to growth at or close to the mean rate for photosynthetic microbes, which is what might be expected for a balanced trophic system. Based in part on the rate estimates from this study, an inverse food web analysis of trophic fluxes suggests that flagellated protists

derive 18–24% of their N from phagotrophy in the upper mixed layer and play a major role in facilitating efficient trophic transfer to larval bluefin tuna in the GoM (Stukel *et al.*, 2021). Direct experimental studies to quantify mixotrophy are consequently an important consideration for future food web investigations in the region.

Growth-grazing imbalance of picoplankton

The mean percent of total phytoplankton production grazed for all GoM cycle profiles ($68 \pm 6\%$ based on FlChl*a*) is consistent with the global average (66%; Steinberg and Landry, 2017). Previous studies in GoM coastal waters have given highly variable results, with microzooplankton grazing accounting for $\leq 50\%$ to $>100\%$ of phytoplankton growth, mainly reflecting the dynamics of bloom increases and declines (Murrell *et al.*, 2002; Juhl and Murrell, 2005; Liu and Dagg, 2005). We expect a less variable coupling of growth and grazing overall for the near steady-state phytoplankton community of the oligotrophic GoM. Such an analysis requires, however, additional information on the grazing contribution of mesozooplankton and is undertaken in Landry and Swalethorp (Landry and Swalethorp, 2021). For picoplankton, however, growth and grazing should be largely balanced within the microbial community that contains the small protistan consumers of picoplankton.

As observed, for example, for PRO and SYN populations in the equatorial and eastern tropical Pacific (Table IV), grazing losses of picoplankton are generally similar to their growth rates, giving a steady-state balance of zero net growth when many rate profiles are averaged over appropriate scales of time and space. Whereas rate imbalances for the Hawaiian lee eddy bloom and adjacent waters of the subtropical Pacific (Table IV) might be dismissed due to small sampling and perturbed system state when studied, our GoM results show consistent growth-grazing offsets for picoplankton over different years and locations (Table II). For PRO, the portion of production grazed varies from 59% (C3) to 77% (C5), with an overall mean of $68.3 \pm 4.3\%$. The euphotic-zone difference between growth and grazing loss averages 0.13 ± 0.2 day^{-1}. For SYN, grazing ranges from 48% (C1) to 89% (C5) of production, with a mean of $66.8 \pm 5.6\%$ and a net rate difference of 0.10 ± 0.2 day^{-1}. For HBACT, $74.1 \pm 5.9\%$ of production is grazed (range = 48 to 86% for C2 and C5, respectively), with a net rate difference of 0.05 ± 0.01 day^{-1}. All averages are significantly different ($P < 0.001$) from the 100% of production grazed and zero net growth rate expected for picoplankton in microbially dominated oligotrophic waters.

One explanation for these imbalances—that picoplankton accumulated in the water parcels studied—can

be rejected based on the net rates of population change calculated from daily sampling profiles following the drifter array. Only PRO exhibited a positive net rate ($+0.04 \pm 0.05$ day^{-1}), but it was both statistically insignificant ($P > 0.48$) and insufficient to account for the average difference in growth and grazing rates observed. Since the net positive growth-grazing rates are measured in the undiluted incubation bottles, they cannot be ascribed to manipulation by dilution or nutrient addition. Similarly, we found no evidence of changes in bead-normalized indices of cell size in initial and final FCM samples that might indicate accelerated cell division rates (more numerous, smaller cells). Unnatural incubation conditions should also not have affected results because the bottles experienced ambient light and temperature.

We suspect that lower grazing on picoplankton arose as a trophic cascade when larger protistan grazers, ciliates and dinoflagellates, were released from the predation pressure of mesozooplankton. In the subtropical Pacific, for example, Calbet and Landry (Calbet and Landry, 1999) found that removal of different size fractions of microbial consumers could alter the net growth rates of PRO by ~ 0.6 day^{-1} and HBACT by ~ 0.2 day^{-1} and that the 5–20 μm fraction had the largest effect on net rates. These cascade effects are four times the net rate differences that would explain our current results. First *et al.* (First *et al.*, 2009) also observed that a model with three interacting groups of protistan consumers could reproduce their results from size-fractioned dilution experiments in the GoM. Given that our experiments started at dawn, large protistan grazers could have grown sufficiently without mesozooplankton predation throughout the day to suppress bacterivory by smaller grazers during the period of intensified nocturnal feeding that often follows synchronized microbial cell division around dusk (Worden and Binder, 2003). We would have measured this as the incomplete removal of the daily bacterial cell production when the bottles were recovered on the following morning. This cascade explanation assumes that mesozooplankton are absent or at unnaturally low concentrations in incubation bottles despite lack of 200-μm pre-screening, presumably because they actively avoid capture in CTD bottles and the suction current during bottle filling. Even at natural abundances, grazing impact of mesozooplankton on phytoplankton is very low in the oceanic GoM, averaging $2 \pm 0.2\%$ of Chl*a* removed per day in our experiments (Landry and Swalethorp, 2021).

Bluefin tuna spawning habitat

In addition to our microbial focus, the present study was conducted with an eye to identifying ecosystem characteristics that might be associated with favorable habitats

for Atlantic bluefin tuna (*Thunnus thynnus*, ABT) larvae in the GoM. Accordingly, our few process studies were not done randomly in the system but targeted locations where an adaptive habitat sampling model, operating with real-time satellite imagery, predicted ABT larvae to be present (Muhling *et al.*, 2010; Domingues *et al.*, 2016). Even so, due to the hit-or-miss happenstance of finding discrete spawning events when adult fish are scarce, only two of the cycles (C1 and C5) sampled water with abundant ABT larvae. What we can say about the microbial characteristics of the larval habitat is therefore limited.

Cycles 1 and 5, the water parcels with abundant larvae, both had origins along the shelf-slope margin of the northeastern GoM (Gerard *et al.*, this issue) but differed substantially in productivity and structure. C1 had the highest growth-production estimates (TChl*a*), the deepest MLD (32 m), and was dominated by eukaryotic groups, led by PRYMN but with higher biomass and rate contributions of DIAT, ADINO and heterotrophic protists than other cycles (Tables I–III). By contrast, C5 productivity was relatively low, the MLD (12 m) was the shallowest sampled and prokaryotes dominated, with notably high contributions of PRO and HBACT. Because both cycles had larvae, we can reasonably conclude that their compositional differences, which also reflect broader differences between 2017 and 2018 cruises, are unlikely to be what matters to or can be sensed by adult tuna when they chose locations to spawn. What C1 and C5 had in common are similar locations of origin (a possible hotspot of spawning activity), the shallowest DCMs of all of the cycles (100 and 78 m, respectively; Table I) and positive growth trends of euphotic zone Chl*a* (Fig. 2). The latter may be more indicative of shelf margin origin, rather than a selected property of spawning sites, but nonetheless could represent an important advective subsidy from the productive margin to the offshore oligotrophic habitats that sustain ABT larvae (Kelly *et al.*, in review). C4, the other cycle with a few ABT larvae present, also showed a Chl*a* increase and shelf-slope margin connectivity (in a different area), but the DCM was deeper (111 m). Chl*a* declined and the DCM was much deeper (120–137 m) for the water parcels, C2 and C3, with no larvae and no recent connectivity to the shelf margin (Gerard *et al.*, this issue).

CONCLUSIONS

Compared to similarly studied open-ocean regions, ABT spawning waters in the oligotrophic GoM have low carbon-based production and low diatom and dinoflagellate contributions to production, although PRYMN can, at least occasionally, rival the more steady importance of *Prochlorococcus* in community dominance. Coupling of phytoplankton growth and microplankton grazing is similar to the global average overall, but stronger in the surface mixed layer than the mid-euphotic zone. Picoplankton growth and grazing processes showed an unexpected large imbalance in experimental incubations, suggesting that the release of large microzooplankton from mesozooplankton predation creates a trophic cascade effect. Despite the limited number of water parcels investigated with and without ABT larvae, our results suggest that small differences within this extreme nutritionally dilute habitat, such as compressed euphotic zones with active mid-layer phytoplankton growth, may be more indicative of the shelf-slope margin locations selected by adult tuna for depositing their eggs than microbial community differences in the offshore habitats where the larvae are transported.

DATA ARCHIVING

Data presented here have been submitted to the National Oceanic and Atmospheric Administration's (NOAA) National Centers for Environmental Information (NCEI) data repository and will also be archived at BCO-DMO (Biological and Chemical Oceanography Data Management Office) site https://www.bco-dmo.org/program/819631.

ACKNOWLEDGEMENTS

FUNDING

REFERENCES

Brown, S. L., Landry, M. R., Selph, K. E., Yang, E. J., Rii, Y. M. and Bidigare, R. R. (2008) Diatoms in the desert; plankton community response to a mesoscale eddy in the subtropical North Pacific. *Deep-Sea Res. II*, **55**, 1321–1333.

Calbet, A. and Landry, M. R. (1999) Mesozooplankton influences on the microbial food web: direct and indirect trophic interactions in the oligotrohic open-ocean. *Limnol. Oceanogr.*, **44**, 1370–1380.

Calbet, A. and Landry, M. R. (2004) Phytoplankton growth, microzooplankton grazing and carbon cycling in marine systems. *Limnol. Oceanogr.*, **49**, 51–57.

Domingues, R., Goni, G., Bringas, F., Muhling, B., Lindo-Atichati, D. and Walter, J. (2016) Variability of preferred environmental conditions for Atlantic bluefin tuna (*Thunnus thynnus*) larvae in the Gulf of Mexico during 1993-2011. *Fish. Oceanogr.*, **25**, 320–336.

Fahnenstiel, G. L., McCormick, M. J., Lang, G. A., Redalje, D., Lohrenz, S. E., Markowitz, M., Wagoner, B. and Carrick, H. J. (1995) Taxon-specific growth and loss rates for dominant phytoplankton populations from the northern Gulf of Mexico. *Mar. Ecol. Prog. Ser.*, **117**, 229–239.

First, M. A., Miller, H. L. III, Lavrentyev, P. J., Pinckney, J. L. and Burd, A. B. (2009) Effects of microzooplankton growth and trophic interactions on herbivory in coastal and offshore environments. *Aquat. Microb. Ecol.*, **54**, 255–267.

First, M. R., Lavrentyev, P. J. and Jochem, F. J. (2007) Patterns of microzooplankton growth in dilution experiments across a trophic gradient: implications for herbivory studies. *Mar. Biol.*, **151**, 1929–1940.

Freibott, A., Linacre, L. and Landry, M. R. (2014) A slide preparation technique for light microscopy analysis of ciliates preserved in acid Lugol's fixative. *Limnol. Oceanogr. Meth.*, **12**, 54–62.

Garrison, D. L., Gowing, M. M., Hughes, M. P., Campbell, L., Caron, D. A., Dennett, M. R., Shalapyonok, A., Olson, R. J. *et al.* (2000) Microbial food web structure in the Arabian Sea: a US JGOFS study. *Deep-Sea Res. II*, **47**, 1387–1422.

Gerard, T., Lamkin, J. T., Kelly, T. B., Knapp, A. N., Laiz-Carrión, R., Malca, E., Selph, K. E., Shiroza, A. *et al.* (this issue) Bluefin larvae in oligotrophic ocean foodwebs, investigations of nutrients to zooplankton: overview of the BLOOFINZ-Gulf of Mexico program. *J. Plankton Res.*

Gifford, D. J. (1988) Impact of grazing by microzooplankton in the Northwest Arm of Halifax Harbour, Nova Scotia. *Mar. Ecol. Prog. Ser.*, **47**, 249–258.

Greer, A. T., Boyette, A. D., Cruz, V. J., Cambazoglu, M. K., Dzwonkowski, B., Chiaverano, L. M., Dykstra, S. L., Briseño-Avena, C. *et al.* (2020) Contrasting fine-scale distributional patterns of zooplankton driven by the formation of a diatom-dominated thin layer. *Limnol. Oceanogr*. **65**, 2236–2258.

Hartmann, M., Grob, C., Tarran, G. A., Martin, A. P., Burkill, P. H., Scanlan, D. J. and Zubkov, M. V. (2012) Mixotrophic basis of Atlantic oligotrophic ecosystems. *Proc. Natl. Acad. Sci. USA.*, **109**, 5756–5760.

Hooker, S. B., Clementson, L., Thomas, C. S., Schlüter, L., Allerup, M., Ras, J., Claustre, H., Normandeau, C. *et al.* (2012) *The Fifth SeaWiFS HPLC Analysis Round-Robin Experiment (SeaHARRE-5). NASA/TM-2012-217503*, NASA, Greenbelt, MD, p. 98.

Jochem, F. J. (2003) Photo- and heterotrophic pico- and nanoplankton in the Mississippi River plume: distribution and grazing activity. *J. Plankton Res.*, **25**, 1201–1214.

Juhl, A. R. and Murrell, M. C. (2005) Interactions between nutrients, phytoplankton growth, and microzooplankton grazing in a Gulf of Mexico estuary. *Aquat. Microb. Ecol.*, **38**, 147–156.

Kelly, T. B., Knapp, A. N., Landry, M. R., Selph, K. E., Shropshire, T. A., Thomas, R. and Stukel, M. R. (in review) Lateral advection supports nitrogen export in the oligotrophic open-ocean Gulf of Mexico. *Nature Comm.*

Knapp, A. N., Thomas, R., Stukel, M. R., Kelly, T. B., Landry, M. R., Selph, K. E. *et al.* (this issue) Constraining the sources of nitrogen fueling phytoplankton and food webs in the Gulf of Mexico using nitrogen isotope budgets. *J. Plankton Res.*

Kranz, S. A., Wang, S., Kelly, T. B., Stukel, M. R., Goericke, R., Landry, M. R. and Cassar, N. (2020) Lagrangian studies of marine production: a multimethod assessment of productivity relationships in the California current ecosystem upwelling region. *J. Geophys. Res. Oceans*. **125**, e2019JC015984.

Landry, M. R., Brown, S. L., Rii, Y. M., Selph, K. E., Bidigare, R. R., Yang, E. J. and Simmons, M. P. (2008) Depth-stratified phytoplankton dynamics in Cyclone *Opal*, a subtropical mesoscale eddy. *Deep-Sea Res. II*, **55**, 1348–1359.

Landry, M. R., Constantinou, J., Latasa, M., Brown, S. L., Bidigare, R. R. and Ondrusek, M. E. (2000) Biological response to iron fertilization in the eastern equatorial Pacific (IronEx II). III. Dynamics of phytoplankton growth and microzooplankton grazing. *Mar. Ecol. Prog. Ser.*, **201**, 57–72.

Landry, M. R., De Verneil, A., Goes, J. I. and Moffett, J. W. (2016a) Plankton dynamics and biogeochemical fluxes in the Costa Rica dome: introduction to the CRD flux and zinc experiments. *J. Plankton Res.*, **38**, 167–182.

Landry, M. R., Ohman, M. D., Goericke, R., Stukel, M. R. and Tsyrkevich, K. (2009) Lagrangian studies of phytoplankton growth and grazing relationships in a coastal upwelling ecosystem off Southern California. *Prog. Oceanogr.*, **83**, 208–216.

Landry, M. R., Selph, K. E., Décima, M., Gutiérrez-Rodríguez, A., Stukel, M. R., Taylor, A. G. and Pasulka, A. L. (2016b) Phytoplankton production and grazing balances in the Costa Rica Dome. *J. Plankton Res.*, **38**, 366–379.

Landry, M. R., Selph, K. E., Taylor, A. G., Décima, M., Balch, W. M. and Bidigare, R. R. (2011a) Phytoplankton growth, grazing and production balances in the HNLC equatorial Pacific. *Deep-Sea Res. II*, **58**, 524–535.

Landry, M. R., Selph, K. E. and Yang, E.-J. (2011b) Decoupled phytoplankton growth and microzooplankton grazing in the deep euphotic zone of the HNLC equatorial Pacific. *Mar. Ecol. Prog. Ser.*, **421**, 13–24.

Landry, M. R., Stukel, M. R. and Décima, M. (2020) Food-web fluxes support high rates of mesozooplankton respiration and production in the equatorial Pacific. *Mar. Ecol. Prog. Ser.*, **652**, 15–32.

Landry, M. R. and Swalethorp, R. (2021) Mesozooplankton biomass, grazing and trophic structure in the bluefin tuna spawning area of the oceanic Gulf of Mexico. *J. Plankton Res.* doi: 10.1093/plankt/fbab008.

Lessard, E. J. and Murrell, M. C. (1998) Microzooplankton herbivory and phytoplankton growth in the northwestern Sargasso Sea. *Aquat. Microb. Ecol.*, **16**, 173–188.

Liu, H. and Dagg, M. (2003) Interactions between nutrients, phytoplankton growth, and micro- and mesozooplankton grazing in the plume of the Mississippi River. *Mar. Ecol. Prog. Ser.*, **258**, 31–42.

Menden-Deuer, S. and Lessard, E. J. (2000) Carbon to volume relationships for dinoflagellates, diatoms and other protist plankton. *Limnol. Oceanogr.*, **45**, 569–579.

Monger, B. C. and Landry, M. R. (1993) Flow cytometric analysis of marine bacteria with Hoechst 33342. *Appl. Environ. Microbiol.*, **59**, 905–911.

Muhling, B. A., Lamkin, J. T. and Roffer, J. T. (2010) Predicting the occurrence of Atlantic bluefin tuna (*Thunnus thynnus*) larvae in the northern Gulf of Mexico: building a classification model from archival data. *Fish. Oceanogr.*, **19**, 526–539.

Murrell, M. C., Stanley, R. S., Lores, E. M., DiDonato, G. T. and Flemer, D. A. (2002) Linkage between microzooplankton grazing and phytoplankton growth in a Gulf of Mexico estuary. *Estuar.*, **25**, 19–29.

Pasulka, A. L., Landry, M. R., Taniguchi, D. A. A., Taylor, A. G. and Church, M. J. (2013) Temporal dynamics of phytoplankton and heterotrophic protists at station ALOHA. *Deep-Sea Res. II Top. Stud. Oceanogr.*, **93**, 44–57.

Putt, M. and Stoecker, D. K. (1989) An experimentally determined carbon: volume ratio for marine "oligotrichous" ciliates from estuarine and coastal waters. *Limnol. Oceanogr.*, **34**, 1097–1103.

Rivkin, R. B. and Legendre, L. (2001) Biogenic carbon cycling in the upper ocean: effects of microbial respiration. *Science*, **291**, 2398–2400.

Selph, K. E., Landry, M. R., Taylor, A. G., Gutiérrez-Rodríguez, A., Stukel, M. R., Wokuluk, J. and Pasulka, A. L. (2016) Phytoplankton production and taxon-specific growth rates in the Costa Rica Dome. *J. Plankton Res.*, **38**, 199–215.

Selph, K. E., Landry, M. R., Taylor, A. G., Yang, E. J., Measures, C. I., Yang, J. J., Stukel, M. R., Christensen, S. *et al.* (2011) Spatially-resolved taxon-specific phytoplankton production and grazing dynamics in relation to iron distributions in the equatorial Pacific between 110 and 140°W. *Deep-Sea Res. II*, **58**, 358–377.

Selph, K. E., Swalethorp, R., Stukel, M. R., Kelly, T. B., Knapp, A. N., Fleming, K., Hernandez, T. and Landry, M. R. (2021) Phytoplankton community composition and biomass in the oligotrophic Gulf of Mexico. *J. Plankton Res.*. doi: 10.1093/plankt/fbab006.

Sherr, E. B. and Sherr, B. F. (1993) Preservation and storage of samples for enumeration of heterotrophic protists. In Kemp, P. K. (ed.), *Handbook of Methods in Aquatic Microbial Ecology*, CRC Press, Boca Raton, FL, pp. 207–212.

Steinberg, D. K. and Landry, M. R. (2017) Zooplankton and the ocean carbon cycle. *Ann. Rev. Mar. Sci.*, **9**, 413–444.

Straile, D. (1997) Gross growth efficiencies of protozoan and metazoan zooplankton and their dependence of food concentration, predator-prey weight ratio, and taxonomic group. *Limnol. Oceanogr.*, **42**, 1375–1385.

Strickland, J. D. H. and Parsons, T. R. (1972) *A Practical Handbook of Seawater Analysis*, Fisheries Research Board, Canada Ottawa.

Strom, S. L. and Strom, M. W. (1996) Microplankton growth, grazing, and community structure in the northern Gulf of Mexico. *Mar. Ecol. Prog. Ser.*, **130**, 229–240.

Stukel, M. R., Girard, T., Kelly, T. B., Knapp, A. N., Laiz-Carrión, R., Lamkin, J. T., Landry, M. R., Malca, E. *et al.* (2021) Plankton food webs in the oligotrophic Gulf of Mexico spawning grounds of Atlantic Bluefin tuna. *J. Plankton Res.*, in press.

Stukel, M. R., Landry, M. R. and Selph, K. E. (2011) Nanoplankton mixotrophy in the eastern equatorial Pacific. *Deep-Sea Res. II*, **58**, 378–386.

Taylor, A. G., Landry, M. R., Freibott, A., Selph, K. E. and Gutiérrez-Rodríguez, A. (2016) Patterns of microbial community biomass, composition and HPLC diagnostic pigments in the Costa Rica upwelling dome. *J. Plankton Res.*, **38**, 183–198.

Taylor, A. G., Landry, M. R., Selph, K. E. and Yang, E. J. (2011) Biomass, size structure and depth distributions of the microbial community in the eastern equatorial Pacific. *Deep-Sea Res. II*, **58**, 342–357.

Unrein, F., Massana, R., Alonso-Sáez, L. and Gasol, J. M. (2007) Significant year-round effect of small mixotrophic flagellates on bacterioplankton in an oligotrophic coastal system. *Limnol. Oceanogr.*, **52**, 456–469.

Valencia, B., Décima, M. and Landry, M. R. (2018) Environmental effects on mesozooplankton size structure and export flux at station ALOHA, North Pacific subtropical gyre. *Glob. Biogeochem. Cyc.*, **32**, 289–305.

Van Heukelem, L. and Thomas, C. S. (2001) Computer-assisted high-performance liquid chromatography method development with applications to the isolation and analysis of phytoplankton pigments. *J. Chromat. A*, **910**, 31–49.

Worden, A. Z. and Binder, B. J. (2003) Application of dilution experiments for measuring growth and mortality rates among *Prochlorococcus* and *Synechococcus* populations in oligotrophic environments. *Aquat. Microb. Ecol.*, **30**, 159–174.

Yingling, N., Kelly, T. B., Selph, K. E., Landry, M. R., Knapp, A. N., Kranz, S. A. and Stukel, M. R. (2021) Taxon-specific phytoplankton growth, nutrient limitation, and light limitation in the oligotrophic Gulf of Mexico. *J. Plankton Res.*, in press.

Zubkov, M. V. and Tarran, G. A. (2008) High bacterivory by the smallest phytoplankton in the North Atlantic. *Nature*, **455**, 224–226.